Aeolian Research 17 (2015) 101–115

Contents lists available at ScienceDirect

Aeolian Research

journal homepage: www.elsevier.com/locate/aeolia

Dust emission and environmental changes in the dried bottom of the Aral Sea

R. Indoitu [a], G. Kozhoridze [a], M. Batyrbaeva [b], I. Vitkovskaya [b], N. Orlovsky [a], D. Blumberg [c], L. Orlovsky [a,*]

[a] Swiss Institute for Dryland Environmental and Energy Research, J. Blaustein Institutes for Desert Research, Ben-Gurion University of the Negev, Sede Boqer Campus, Midreshet Ben-Gurion 84990, Israel
[b] Department of Earth Monitoring, National Centre of Space Research and Technology of Kazakhstan, Shevchenko St. 15, Almaty 050010, Kazakhstan
[c] Department of Geography, Ben-Gurion University of the Negev, Beer-Sheva 84105, Israel

ARTICLE INFO

Article history:
Received 25 June 2014
Revised 25 February 2015
Accepted 25 February 2015
Available online 22 March 2015

Keywords:
Dust storms
Remote sensing
Aerosol index
Land-cover changes
Desertification

ABSTRACT

In the 1990s, the western world became aware of the ecological disaster of what was once the fourth largest lake in the world – the Aral Sea. The drastic desiccation of the Aral Sea led to the intensive development of desertification processes in the region and the formation of a new desert, the Aralkum. In the last few decades, the Aralkum has become the new "hot spot" of dust and salt storms in the region. Dust storms and their source areas have been determined and analyzed by the NOAA AVHRR, TOMS and OMI data. An analysis of the land-cover changes in the dried bottom of the Aral Sea revealed that the north-eastern part of the Aralkum Desert is one of the most active dust sources in the region, responsible for high aerosol concentrations in the atmosphere. Dust plumes that sweep up from the dried bottom of the Aral Sea have become larger, and dust storms have become more powerful, since the bottom exposure. The main change that occurred in the land cover was the considerable reduction of vegetation and small water bodies, while the areas of solonchaks (salty pans) and sandy massifs increased significantly.

1. Introduction

In the 1990s, the western world became aware of the ecological disaster occurring at the fourth largest lake in the world – the Aral Sea. The demise of the Aral Sea has been called one of the 20th century's worst environmental catastrophes and has been referred to as a "quiet Chernobyl" (Glantz and Figueroa, 1997). The drastic desiccation of the Aral Sea led to the intensification of desertification processes in the region and the development of a new desert, the Aralkum, on the dried sea bottom. In the last few decades, the exposed bottom has become the new "hot spot" of dust and salt storms in the region.

The drylands of Southern Kazakhstan, Uzbekistan and Turkmenistan have always been affected by hazardous dust storms. In the last thirty years of the 20th century, however, the dust storm activities showed a significant downward trend over the entire region (Indoitu et al., 2012). In contrast, the Aral Sea region has shown a major increasing trend in dust storms' strength and frequency (Spivak et al., 2012). In the absence of the conventional system of dust storm monitoring – there are no meteorological stations established on the dried bottom of the Aral Sea, *and the meteorological station on Vozrojdenie Island was closed in 1992* – the only source of information is remote sensing.

Remotely sensed data from satellite-based platforms such as the Advanced Very High Resolution Radiometer on-board the NOAA Polar Orbiting Environmental Satellite (NOAA AVHRR), the Total Ozone Mapping Spectrometer (TOMS) on the Nimbus and Earth Probe platforms, METEOSAT, the Geostationary Operational Environmental Satellites (GOES) series, the Sea-viewing Wide Field-of-view Sensor (SeaWiFS), and the Earth Observing System's MODerate resolution Imaging Spectroradiometer (MODIS) monitor and collect data regarding dust emission sites and trajectories of dust aerosol movement (Chavez et al., 2002; Fan Yi-da et al., 2001; Prospero et al., 2002). The above listed high temporal resolution data as well as moderate spatial resolution data such as Landsat and SPOT are widely used for dust storms studies.

In most cases, the satellite images capture clouds near the dust plumes, which consequently, create difficulties in differentiating the two. Many researchers have shown that to be able to distinguish between clouds and dust aerosol, it is necessary to display the images in VIS- and IR-band combinations and to pay close

* Corresponding author. Tel.: +972 8 6596857; fax: +972 8 6596921.
E-mail address: orlovsky@bgu.ac.il (L. Orlovsky).

http://dx.doi.org/10.1016/j.aeolia.2015.02.004
1875-9637/

attention to the specific dust plume structures. False color images with an RGB combination of the 1, 2, and 4 bands show the dust plumes in a light yellow–brownish color, and clouds in a bright yellow color (Rivera et al., 2006). Janugani et al. (2009) showed that a band combination of 1, 4, and 5 for the colors red, green, and blue of the 5-band NOAA-AVHRR imagery was probably the best one with which to locate the dust sources during visual interpretation. Miller (2003) proposed using the combination of MODIS bands 1, 3, 4 and 26 in the visible spectrum and infrared bands 31–32 to discriminate dust loads from clouds and the desert background.

Several techniques have been developed to detect dust storms based on visible and thermal infrared satellite data: band math analysis, differencing of radiation temperature or the infrared split-window technique (BTD), single band thresholding and multi-band combinations (Ackerman, 1989, 1997; Janugani et al., 2009). Recent studies have demonstrated the efficiency of using thermal bands for monitoring dust aerosol outbreaks (Hu et al., 2008). An effective method for detecting and differentiating dust from clouds using satellite remote sensing has been the brightness temperature difference (BTD) of NOAA/AVHRR channel 4 and channel 5 (Chavez et al., 2002; Janugani et al., 2009; Tsolmon et al., 2008; Prospero, 1999). The BTD of the two bands can distinguish not only a dust storm but also the density of dust and sand in the moving mass (Tsolmon et al., 2008).

Dust particles produce specific emissivity characteristics in the VIS (8.6 μm)–NIR (11 μm) and NIR (11 μm)–TIR (12 μm) bands. In the first spectral range the dust particles create brightness temperature differences similar to those of thin cirrus clouds (Roskovensky and Liouand, 2005), whereas in the second spectral range the BTD is negative because dust has a higher emissivity at 12 μm than at 11 μm (Huang et al., 2007). At the same time, the thermal infrared spectrum of minerals strongly depend on the particle size and there is a temperature difference between the surface and the dust aerosols in the air (Hu et al., 2008). A negative BTD is mainly caused by the silicate absorption of the shorter wavelengths, while the ice and water particles absorb longer wavelengths (Li et al., 2010).

Data from different sensors show a good consistency both in the long and the short term. A comparison of TOMS data with other sources of information (METEOSAT/VIS) demonstrates that in spite of certain limitations of the former, such as a low spatial resolution of 50×50 km and probable cloud contamination at the sub-pixel level, both datasets are consistent and allow for the analysis of dust loads at regional and global scales (Chiapello and Moulin, 2002; Chiapello et al., 2005). Evan et al. (2006) compared data from the Aerosol Robotic Network (AERONET), METEOSAT and TOMS over the North Atlantic to test the algorithm for dust detection over water and found that long-term AVHRR imagery plays an important role in the study of airborne dust. Narrowband satellite sensors (e.g. AVHRR, HIRS, MODIS, GOES) allow dust load detection, while higher spectral resolution imagery is necessary to quantify dust characteristics (Sokolik, 2002). Tsolmon et al. (2008) analyzed the potential of MODIS and AVHRR data for monitoring and mapping dust storms in Mongolia and northern China, and found the synergy between these two sources of information. Data from OMI coincident with events detected by other sensors have been widely used for tracking the dust trajectories. Jafari and Malekian (2015), who compared five different dust detection algorithms using MODIS data and collated them with OMI AI maps, revealed a high correlation between both products over water and desert surfaces.

Previous studies confirmed that the aerosol index (AI) values of NASA TOMS can be used to map the spatial and temporal distributions of atmospheric aerosols, and correspondingly, the dust storm sources (Engelstaedter et al., 2006; Prospero et al., 2002; Washington et al., 2003). According to the AI values determined by TOMS, the most active dust-producing areas are connected to large dried lake basins: the Tarim Basin in China, the Lake Eyre Basin in Australia, the Salar de Uyuni in Atacama, Chile, and the Great Salt Lake Desert in the USA (Washington et al., 2003). The key dust source in the world is the Bodélé Depression, in northern Chad, which is a shallow basin of exposed diatomite sediment, much of which was deposited under the paleolake Megachad some 7000 years ago when it was the biggest lake on the planet (Washington et al., 2003, 2009).

The drylands of Central Asia experience dust storms with frequencies that are among the highest in the world (Orlovsky et al., 2005). The appearance of additional vast area prone to wind erosion namely anthropogenically created Aralkum Desert had inevitably led to the activization of dust emission processes.

Prior to the modern recession, the Aral Sea experienced a number of water level declines and subsequent recoveries over the last 10 thousand years (Micklin, 2010; Singh et al., 2012). Recessions and advances of the sea waters resulted from major changes in the river discharge into it, caused by significant climatic changes, and during the past 3000 years, also by human activities (Micklin, 1988).

In modern times, the Aral Sea's ecological disaster was the result of the USSR government's decision, in the 1960s, to undertake an agricultural project for increasing cotton production in Soviet Central Asia. The expansion of irrigated fields resulted in a drastic reduction of the water volume discharged into the lake. In 1960, the water flow from the Amudarya and Syrdarya Rivers, which represented the major input for the Aral Sea, varied from 56×10^9 m^3/year to 60×10^9 m^3/year (Orlovsky and Orlovsky, 2001); by the mid-1980s, the water flow had almost ceased, and the water volume discharged was 3.5×10^9 m^3/year (Saiko and Zonn, 2000). By 2007 the water inflow to the Aral Sea was about 5×10^9 m^3/year -10×10^9 m^3/year (Dukhovny and Stulina, 2011). The lake has progressively shrunk due to a lack of recharge by the rivers and high evaporation during summer time. By 1999, the lake level had dropped by 18 m, down to the mark of 33.8.m MSL (Orlovsky and Orlovsky, 2001). Following the division of the Aral Sea in 2005, the salinity level in the Large Aral increased by as much as 90 g/l (western part, depth 21 m) and 160 g/l (eastern part, depth 28.3 m), while in the Small Aral, it decreased and reached 17 g/l (Aladin et al., 2009). By 2009, the Aral Sea was divided into three separate water bodies: the Small Aral, which has been restored after the construction of a dam in 2005; the western part of the Large Aral adjacent to the Ustyurt Plateau; and a little pond that appears during rainy seasons in the eastern part of the former Large Aral.

The glaciers from the surrounding mountain chains are the main providers of the water flow for the two major Central Asian rivers: the Syrdarya and the Amudarya. Rising (due to climate change) temperatures have been melting Central Asia's glaciers. The Pamir-Alai glaciers lost 19% of their mass during the second half of the 20th century (Perelet, 2008). The glaciers in the Tien Shan Mountains cover a surface of over 15,000 km^2, which in recent decades, have been losing between 0.1% and 0.8% of their surface per year (Sorg et al., 2012). The intensive melting of the glaciers in the last fifty years has reduced the water flow into the Amudarya and Syrdarya Rivers, contributing, as well, to the desiccation process of the Aral Sea.

These multiple changes have had an enormous environmental impact. The territory was proclaimed an "ecological disaster zone" (Saiko and Zonn, 2000). The critical transformations in the hydrometeorological regime of the Aral Sea has led to soil degradation and the desertification of immense areas (Orlovsky et al., 2004).

Studies of natural ecosystems executed during the 1960s-1990s showed that the desiccation of the sea affected micro- and

meso-climates in the region. In the last few decades significant temperature increases during summer time and decreases in winter values have been recorded (Novikova, 2004). Increases in extreme air temperatures (Micklin, 1988), as well as in the amplitudes of mean daily, monthly and annual values have been observed (Khan et al., 2004). Kozhoridze et al. (2012) showed that at the Aralsk Meteorological Station, located in the northeastern Aral Sea, there has been a significant increasing temperature trend of approximately 0.02 °C/year during the last century.

For millions of years, the Aral Sea received the salts of the Aral Basin, and for the last four-five decades, it has served as a repository of the fertilizers, pesticides, herbicides and other chemicals washed away from the irrigated massifs of the region (Dedova et al., 2006; Galaeva and Idrysova, 2007; Orlovsky and Orlovsky, 2001). Nowadays, the exposed bottom of the sea has become the "distributer" of salts and chemicals over the adjacent areas. Thus, the salt storms, also referred to as "white dust storms" (Orlovsky and Orlovsky, 2001), have brought about the serious pollution of the air, soil, water and agricultural products, as well as causing a variety of diseases and the degradation of natural ecosystems. From 1960 to 1984 the amount of salts and other toxic particles carried annually from the dried bottom of the Aral Sea to distances of hundreds of kilometers by different estimations varied from 15 million metric tons to 75 million metric tons, and raised considerable concerns about the impact on human health (Glantz, 1999; Saiko and Zonn, 2000). Estimates of the total transported by wind material, which were made in the late 1980s, ranged from 13 million metric tons per year to as high as 231 million metric tons per year (Glazovskiy, 1990). At any rate, over 57,500 km^2 of the former seabed has been exposed (Indoitu et al., 2012), and the dried bottom of the sea is being turned into a powerful source of dust and salt emissions (Galaeva and Idrysova, 2007; Wiggs et al., 2003). The main objectives of the present paper were (1) to monitor the dust events originating from the dried bottom of the Aral Sea using NOAA-AVHRR imagery, TOMS and OMI AI maps and (2) to reveal the active dust emission sites in the study area.

2. Remote sensing monitoring of dust storms in the Aral region in the 1970s–1980s

Starting in the 1970s, satellite images became available for monitoring the sea's water regression and the dust events in the Circum-Aral region (Priaralye in the Russian language literature). Over the years, these remote sensing methods successfully illustrated the shrinking of the sea (Fig. 1).

The first dust storms in the Circum-Aral region were registered in the spring of 1975 by the Meteor and NOAA satellites (Grigoryev and Lipatov, 1983). These were the first remote sensing observations that revealed the huge size of dust plumes stretching for tens of kilometers in length (Kondratyev et al., 1985).

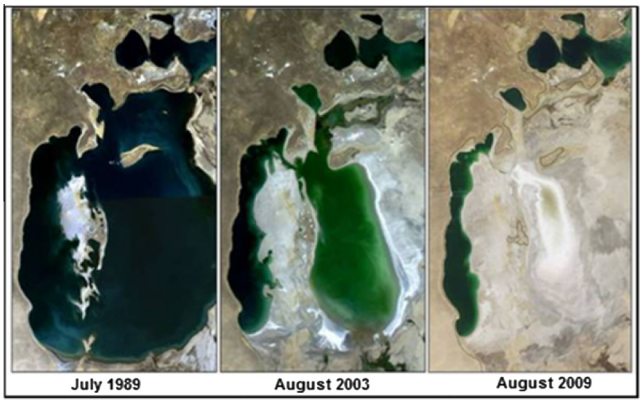

Fig. 1. Drying of the Aral Sea through time (NASA Earth Observatory).

The first dust storm source area, observed in the images taken in 1975, was detected on the adjacent sea terrace in the northeastern and eastern regions of the Aral Sea, which started appearing back in 1961, and by the time the image was taken, its width was about 20–25 km and the area of the dried bottom was 3000 km^2 (Grigoryev and Lipatov, 1982; Kondratyev et al., 1985). In 1982, Grigoryev and Lipatov mentioned that the northeastern source area had a width of 30–45 km with a maximum of 50 km, and the length of the dust plumes was, on average, 125 km. In 1990, the dust-forming source areas of the eastern seashore reached to more than 10,000 km^2 (Grigoryev and Jogova, 1992).

By 1982, also using satellite images, the second significant dust source area was observed around the dry sea bottom of Vozrojdenie Island, with an area of 2000 km^2. Several years later, in 1989, the satellite images showed a third minor (200 km^2) dust-forming source on the northwestern side of the sea – on the Kulandy Peninsula (Grigoryev and Jogova, 1992).

The image analysis of 1990 showed the increased surface of the dry bottom of the Aral Sea (29,000 km^2) and revealed new dust source areas on the southeastern shore of the Large Aral and on the eastern shore of the Small Aral (Grigoryev and Jogova, 1992). The dry belt of the southeastern shore reached widths of 30–50 km.

According to the satellite imaging, the dust plumes could stretch for lengths of 150–300 km, with a maximum of 500 km (May 6, 1979) (Grigoryev and Lipatov, 1983; Kondratyev et al., 1985; Grigoryev and Jogova, 1992). The first estimations of the dust volumes transported during the dust storms in 1975 were, on average, 45 million metric tons per year (Grigoryev and Lipatov, 1983), while in 1990, this figure doubled (90 million metric tons per year) (Grigoryev and Jogova, 1992). In addition to the fine grains carried from the sandy and solonchak surfaces, the dust plume loads contained salts, as sulfates and chlorides, which were deposited over an area of 250,000 km^2 (Kondratyev et al., 1985).

Kaypov et al. (2012) analyzed a NOAA AVHRR image, taken on April 28–29, 2008, which captured a large dust event that originated on the eastern desiccated seabed. The authors learned that this particular dust storm lifted from the ground and carried away 2.6 million metric tons of silt particles of 50 μm diameter, and 5.4 million metric tons of silt particles of 35 μm diameter. Particles of PM10 were carried away to distances of 1400 km, reaching northern Iran and western Turkmenistan.

The monitoring of dust storm outbreaks, over the new developing desert on the dry bottom of the sea, revealed that the temporal distribution of the dust storm events increased significantly. The long-term remote sensing data analysis, for the period from 1975 to 1982, showed a total of 37 dust storm events; from 1985 to 1990, 33 dust storm outbreaks were recorded (Grigoryev and Jogova, 1992). From 1990 to 2002, the measurements executed at nine meteorological stations in the Circum-Aral region registered 1082 days with dust storms of different intensities and durations (Shardakova and Usmanova, 2006).

Grigoryev and Lipatov (1983), in their analysis of satellite images for the years 1975–1981, revealed three main directions of the dust plume flows. In 60% of the cases, dust storms were toward the southwest, and 25% to the west and the remaining 15% moved toward the south and southeast. The images of 1975 showed that the dust plume almost never reached the western shore of the Sea (Grigoryev and Lipatov, 1983), instead mainly falling out on the water surface (Kondratyev et al., 2002). However, during the dust outbreaks of 1979, most of the dust plumes reached the adjacent shore, most frequently on the south and southwestern shores (Kondratyev et al., 2002).

As the water body retreated, new dust "hot spots" appeared. It has been believed that the "old" dried bottom surface, which dried

before the 1990s, hasn't been, in the last decades, an active source of dust and salts due to desalination and intensive colonization by vegetation (Dosbergenov and Asanbayev, 2002). Thus, there have been claims that the "new" dried sea bottom areas are the only active dust zones, while the "old" areas of the drying sea have lost their significance as active dust source areas (Semenov, 2011). Our suggestion is that the "old" dried sea surfaces continue to be active dust emission sites along with the newly exposed sea bottom.

3. Methods and data

3.1. NOAA AVHRR images

NOAA/AVHRR (12, 16 and 18) images were used in order to recognize the sources, the paths and the transformations of the dust events in the Aral Sea region from 2005 to 2008. The Advanced Very High Resolution Radiometer (AVHRR) is a multipurpose imaging instrument used for the global measurement of cloud cover, sea surface temperature, ice, snow, vegetation cover and large meteorological events (NESEDIS: NOAA Satellite, 2011). AVHRR has five channels in the visible and infrared spectra between 0.63 and 12.0 micrometers (band 1 VIS 0.58–0.68 mm; band 2 NIR 0.73–1.10 mm; band 3 MIR, 3.55–3.93 mm; bands 4 and 5 TIR10.3–11.3 mm and 11.5–12.5 mm), with a resolution of 1.1 km at the sub-satellite point and high temporal resolutions (once per day). Monitoring of dust storms from 2005 to 2008 had been done on a daily basis at the Telonics NOAA AVHRR Receiving Station at the Department of Earth Monitoring of the National Centre of Space Research and Technology of Kazakhstan (formerly the Space Research Institute), in Almaty, Kazakhstan in the framework of the collaborative research project CALTER granted by the European Commission.

The process of acquiring, processing and archiving the low spatial resolution imagery includes the following stages:

- Planning of the survey and receiving the raw data.
- Preliminary processing of the satellite data and obtaining the basic files. The processing was carried out using the mathematical package of the Telonics Receiving Station. The exit data are in RAW-format.
- Secondary processing and obtaining HDF-files. This stage includes processing images using CAPS (Common AVHRR Processing Software). CAPS supports the following five functions: (1) operations on processing the data; (2) reading HRPT-data (High Resolution Picture Transmission) from AVHRR; (3) reading and writing HDF files; (4) converting radiometer data into values of radiance, reflectance, and brightness temperature; and (5) georeferencing of the satellite data to standard geographic projection. The result of this stage are files in HDF-format allowing further analysis.

A database of the images with 1.1 km spatial resolution for the territory of the Circum-Aral region was created. Monitoring of the dust storms was carried out in the polygon within coordinates 56–64 °E and 42–48 °N, projection Lat/Lon for spheroid WGS 84.

Images taken around 14:00 h local time have been pre-viewed, and the "suspicious" (from the dust storm viewpoint) images have been selected. In order to distinguish between clouds and dust event, every image was displayed in VIS and IR band combinations and every dust storm plume was identified by specific structure and color. False color images with an RGB combination of 1, 2, 4 bands showed the dust plumes in light yellow–brownish color, and clouds in a bright yellow color. Bands combination 1, 4, 5 for colors Red, Green, and Blue was very efficient to locate the dust sources during visual interpretation, as well. The multi-spectral images consisting of five spectral bands (visible, near-infrared, and three thermal infrared channels) have been "built" and copied to CD/DVD for further processing and interpretation.

To assure that the selected images demonstrate dust events, the Brightness Temperature Difference (BTD) procedure was applied (Janugani et al., 2009):

$$BTD = ch4 - ch5 \quad (1)$$

where ch4 for AVHRR is between 10.3 μm and 11.3 μm, and ch5 between 11.5 μm and 12.5 μm.

For the period from 2005 to 2008 dust storms originating from the dried bottom of the Aral Sea were identified in a total of 42 images. These images were used for: (1) to define the borders of the dried bottom of the Aral Sea for 2005–2008, and (2) to determine the directions of dust transportation, approximate area and length of dust plumes during each event, and dust source areas. The water border of the 1999 Aral Sea was downloaded as a shape file from Google Pro. For this purpose Arc GIS and ERDAS IMAGINE software was used. The following analysis included defining the borders of the dust plumes and the limits of the dust emission sites, along with an assessment of the intensity of emission. Image processing included two stages (after identification of the dust storm event in the image). The first stage involved detecting the borders of the emission zone with an assessment of the emission intensity inside. The local level of atmospheric turbidity, stipulated by the rise of aerosols, and the specific texture of dust loads above emission sites were taken as characteristics of intensity. Mathematically, the emission zone and the distribution of wind erosion intensity inside were expressed as a system of graph nodes (points of graph): the higher density of depicted nodes reflects the higher intensity of emission (Spivak et al., 2009). In the second stage, the series of nodes were mathematically processed in order to determine the contour of the emission zone using the algorithm of a minimally tight tree. Median filtering was applied for calculating the node density matrix, which characterizes the intensity of wind erosion (Spivak et al., 2009).

3.2. TOMS and OMI AIs

To show the aerosol concentration of the dust plumes over the exposed Aral Sea bottom and adjacent areas, the TOMS (Total Ozone Mapping Spectrometer) and OMI (from Aura's Ozone Monitoring Instrument) aerosol indices (AI) were used as an additional tool. The aerosol index (AI) is a calculation of the difference between the amount of ultraviolet (UV) light that the dust-filled atmosphere scatters back to the satellite and the amount of UV the atmosphere would scatter back if the skies were totally clear (Hickey and Goudie, 2007). The AI shows absorbing aerosols over the land surface and water, thus making possible the observation and tracing of large dust events (Hickey and Goudie, 2007). Positive values of the AI generally represent absorbing aerosols (dust and smoke), while small or negative values represent nonabsorbing aerosols and clouds. We believe that in the study area the aerosols consist mainly of dust, since vegetation on the dry sea floor is very sparse (Breckle et al., 2012; Novikova, 2004) and if put on fire wouldn't have the power to produce such large and massive smoke plumes. The other monitored and modelled data confirm our assumption (Elguindi and Giorgi, 2007; Putman, 2012).

The TOMS and OMI AIs were used to map the daily, monthly and annual averages of aerosol concentrations over the Aral Sea and adjacent areas.

The UV Aerosol Index from the Nimbus 7 TOMS for 1980–1990, and Earth Probe TOMS data from 1997 to 2004, retrieved from the TOMS Online Visualization and Analysis database (GIOVANNI: http://gdata1.sci.gsfc.nasa.gov/daac-bin/G3/gui.cgi?instance_id=toms), were

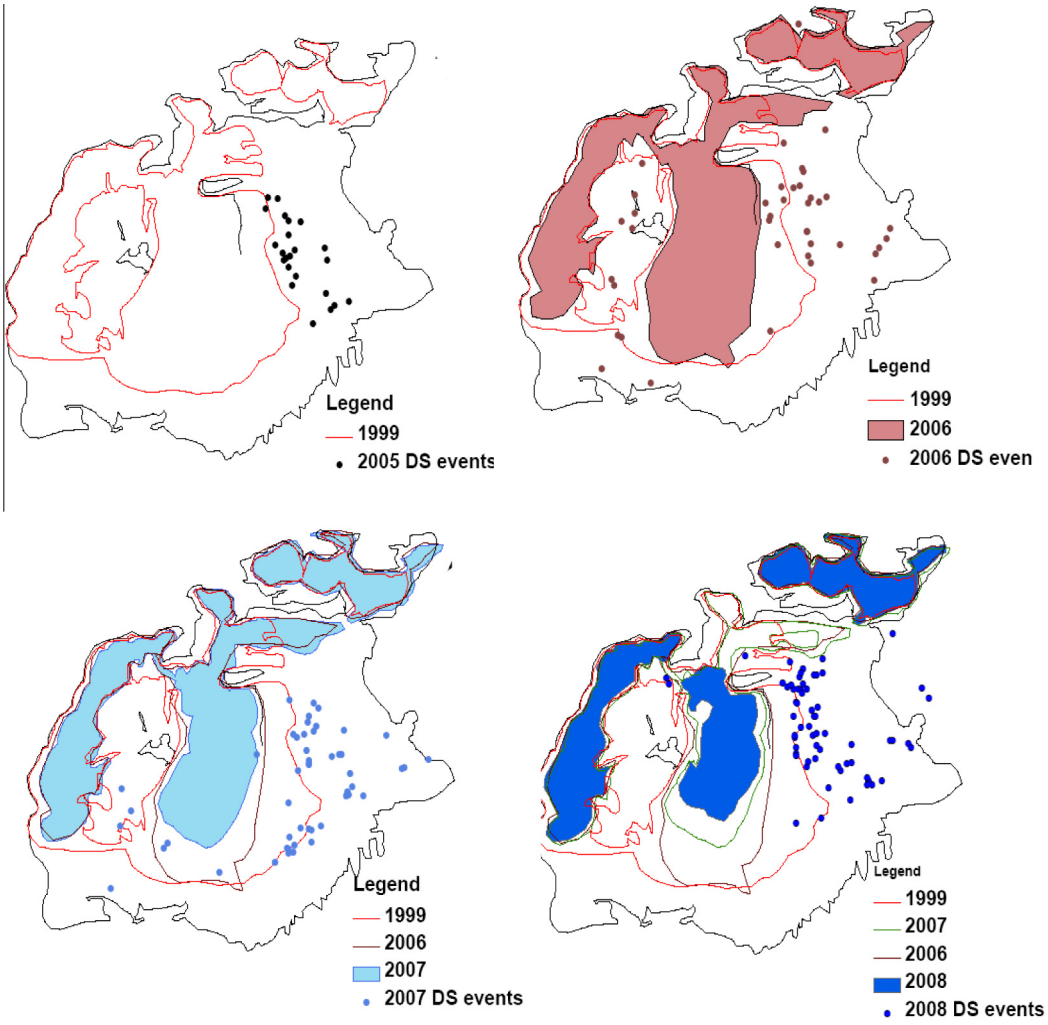

Fig. 2. Dust storm sources on the dried bottom of the Aral Sea (2005–2008).

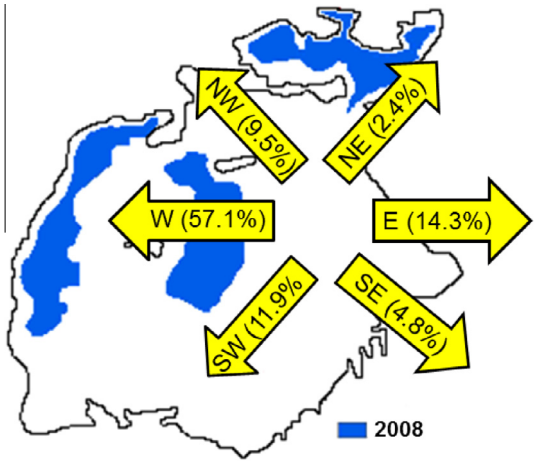

Fig. 3. Direction of dust storm plumes during 2005–2008.

used to demonstrate the seasonal (March–September) aerosol concentrations from 1980 to 2004.

The maps of mean annual aerosol concentrations from 2005 to 2010, monthly and annual averages for 2005–2008, and daily data for selected dust events from 2005 to 2008 were created using OMI AI data. OMI AI (OMTO3d Surface UV) data were retrieved using the OMI/Aura Online Visualization and Analysis tool with daily Level 3 Global Gridded products (GIOVANNI: http://gdata1.sci.gsfc.nasa.gov/daac-bin/G3/gui.cgi?instance_id=omi). Guidelines for data download and use are described in details by Acker and Leptoukh (2007).

The Digital Elevation Model of the dried bottom of the Aral Sea with a spatial resolution of 90 m was produced from www.worldclim.com and http://srtm.csi.cgiar.org/).

4. Results and discussion

4.1. Dust storm analysis using NOAA AVHRR data

One of the hypotheses of this research was that despite the fact that the "old" dried seabed is becoming covered with patches of sparse vegetation, it remains an active dust storm source along with the "newer" dried seabed. From 1975 to 1981, the main source area was the eastern shore of the Aral Sea where 60% of the dust storms were toward the southwest, and 25% toward the west and the remaining 15% moved toward the south or southeast (Grigoryev and Lipatov, 1974). Fig. 2 demonstrates the expert assessment of the dust sources based on the NOAA AVHRR images from 2005 to 2008. The spatial distribution of the source points in 2005–2008 (Fig. 2) indicates that the "old" dried seabed appeared before 1990, and since 2000, it has been a strong dust source area until the present. The 1999 sea water line was used as the

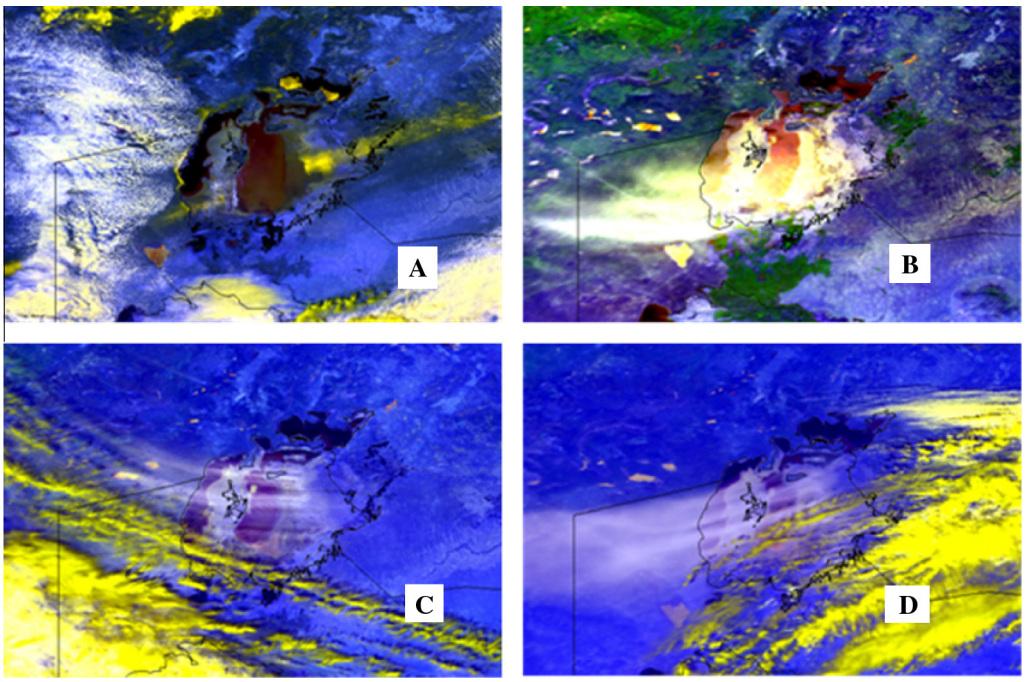

Fig. 4. Dust storm plumes of different structures rising from the Aral Sea dried surfaces. (A) 03.04.2005 (band:1,2,3); (B) 29.05.2007 (band:1,2,4); (C) 18.04.2008 (band:1,2,4); (D) 29.04.2008 (band:1,2,4).

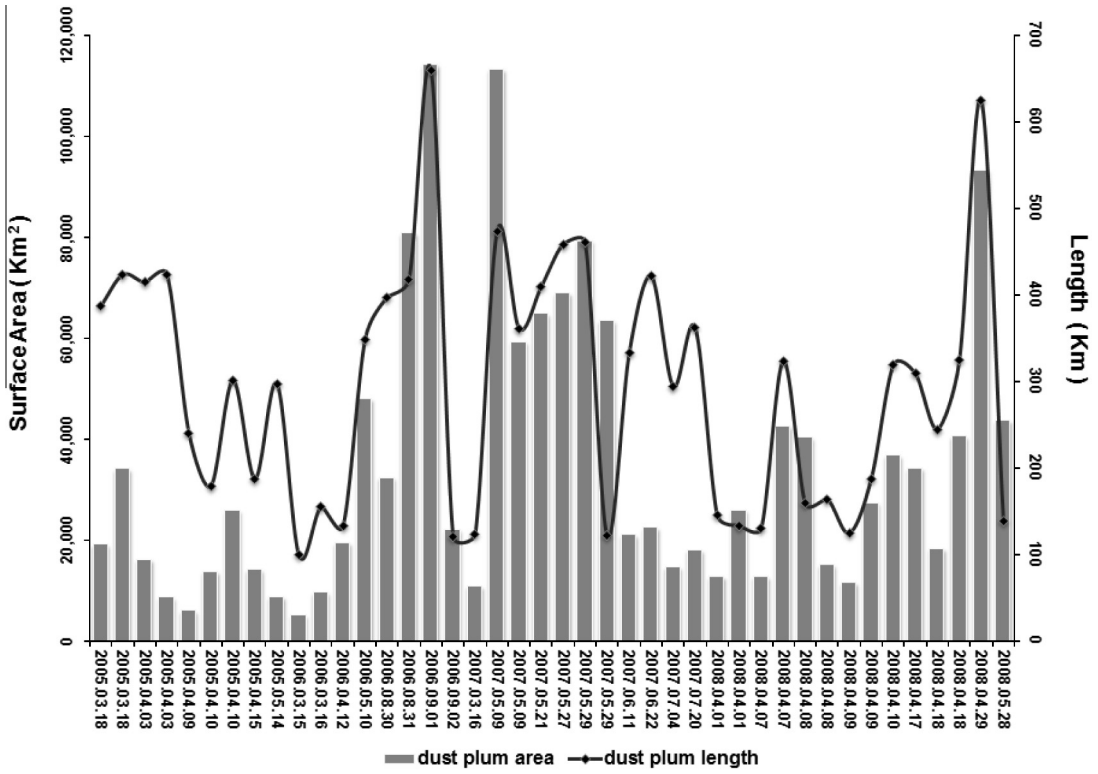

Fig. 5. Approximate estimate of dust plumes parameters measured by NOAA-AVHRR images in 2005–2008.

reference border for the "old" dried sea bed. From the available forty-two NOAA AVHRR images, a total of 30 dust events of different durations, sizes and structures were counted, from which about 70% occurred on the "old" dried seabed.

Six days with dust storms were observed in the NOAA/AVHRR images in 2005, with all events originating on the northeastern shore (see Fig. 2). During 2006 and 2007, nine days with dust events were observed each year, and in both years, dust plumes rose from the entire eastern and southern dry seabed (see Fig. 2). Additionally, during 2006 and 2007, dust was blown from the Vozrojdenie Peninsula, which has been a completely dried sandy surface for a long time. It is noticeable that the dust plumes were

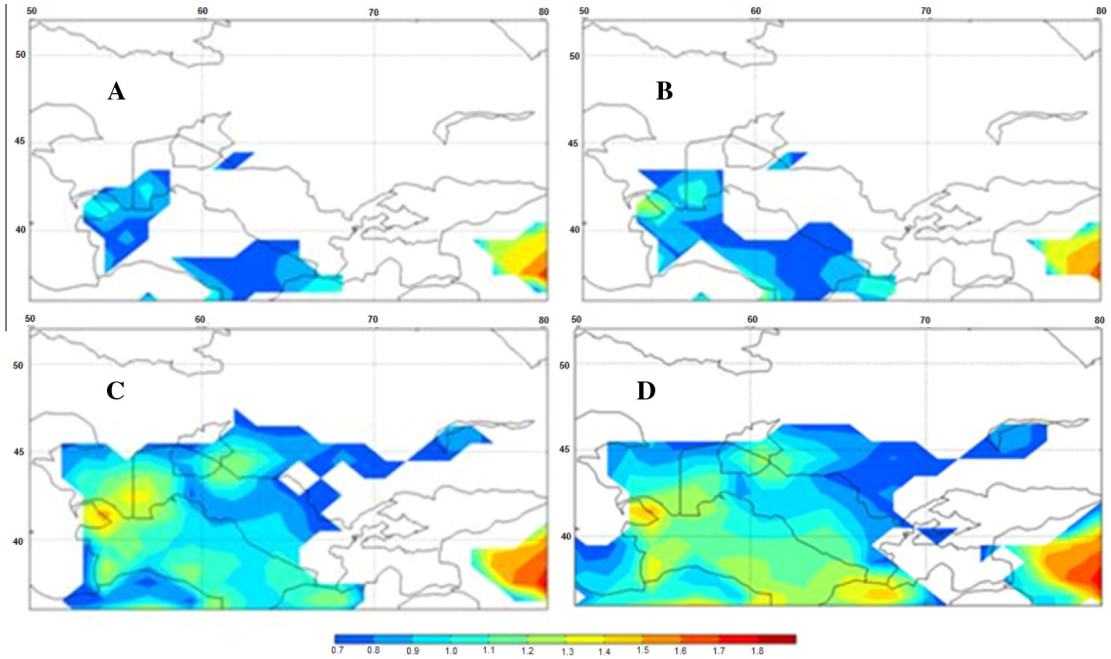

Fig. 6. Spatial pattern of TOMS dust concentrations in the Aral Sea basin during March–September, through: (A) 1980–1985; (B) 1986–1990; (C) 1997–2000; (D) 2000–2004 (retrieved from TOMS Online Visualization and Analysis database (GIOVANNI: http://gdata1.sci.gsfc.nasa.gov/daac-bin/G3/gui.cgi?instance_id=toms).

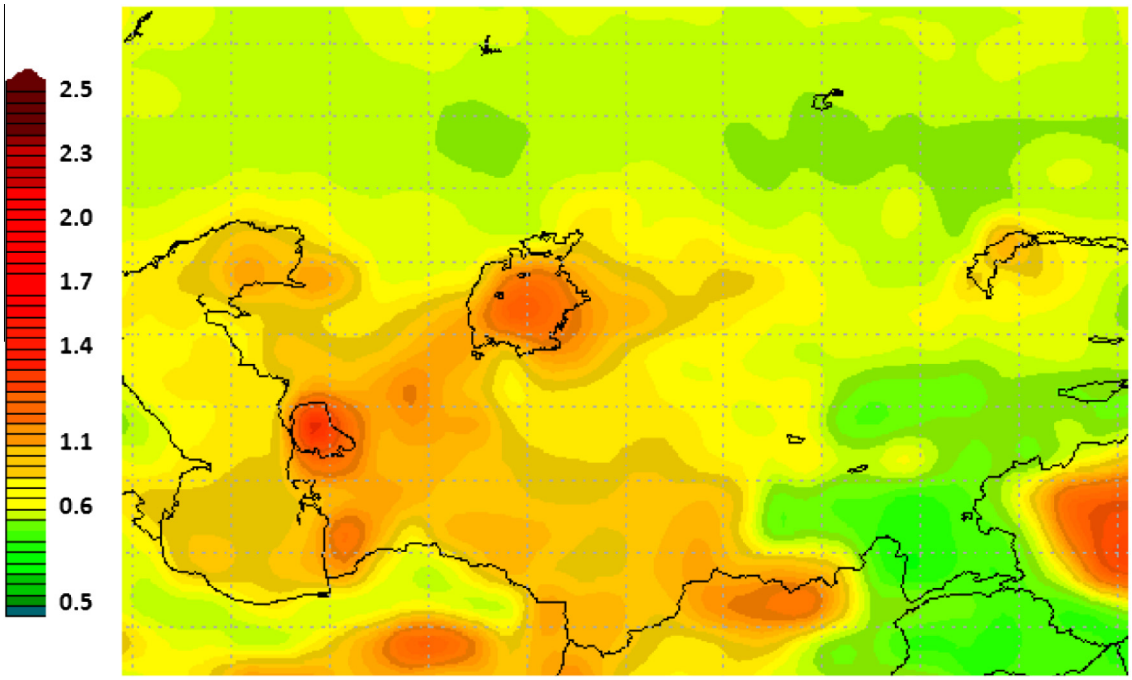

Fig. 7. OMI AI average for 2005–2010 (March–September) (retrieved from OMI/Aura Online Visualization and Analysis tool with daily Level 3 Global Gridded products (GIOVANNI: http://gdata1.sci.gsfc.nasa.gov/daac-bin/G3/gui.cgi?instance_id=omi).

blown from both the "older" dried sea bottom and from the "newer" dried areas. In 2008, NOAA AVHRR registered at least nine days of dust storms in the Aral Sea's dried bottom. The dust storm outbreaks were spotted on the "older" and "newly" dried north-eastern terraces of the sea (see Fig. 2).

The area of the Aral Sea's dried bottom was estimated to be about 34,000 km^2 in 2006. In the following years, the water surface continued to shrink, and the Aralkum Desert expanded to about 38,000 km^2 in 2007, 44,000 km^2 in 2008, and more than 57,000 km^2 in 2011 (see Fig. 2).

From 2005 to 2008, the dust sources were detected on the eastern and southern shores, and on the Vozrojdenie Peninsula. Dust plume flows were registered during these four years mainly toward the west (57.1%) and only 11.9% toward the southwest (Fig. 3). Dust storm plumes were also captured rising from the eastern shore and flowing toward the east (14.3%).

An analysis of the NOAA AVHRR images revealed that there were two types of dust plume emissions: either one large dust plume or many small dust plumes. In most cases, a large dust plume was accompanied by numerous smaller plumes. Large

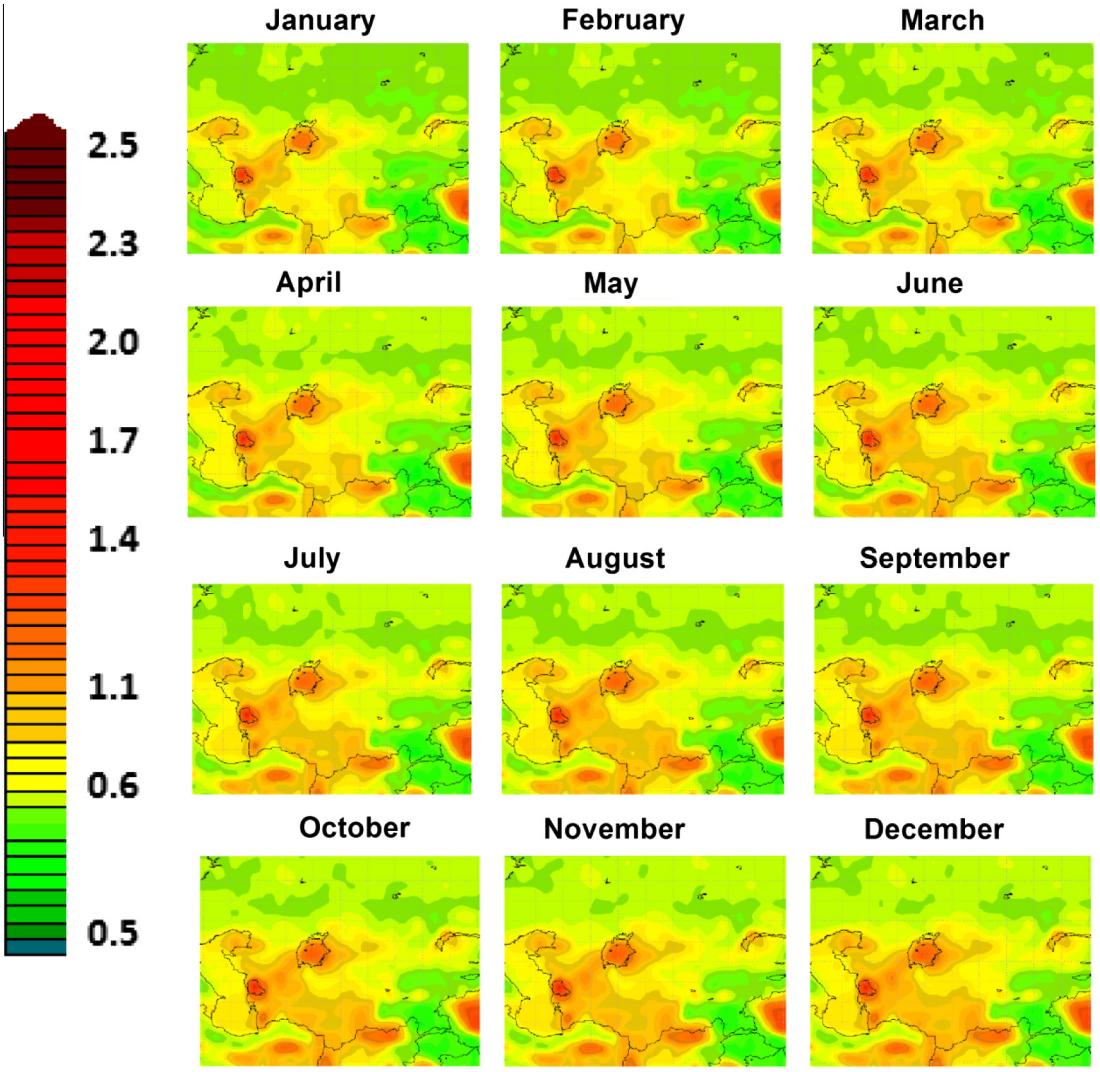

Fig. 8. Monthly average (2005–2008) of aerosol index (AI) over Middle Asia retrieved in the ultraviolet by OMI (January–December).

macrostructure dust plumes rose only from the seabed dried before 1999 where the surface was perfectly dried up, i.e., the eastern and southeastern shores. This type of dust plume had a width of up to 60–100 km (Fig. 4). Each small dust plume had a width of over 5–20 km (Fig. 4A–D). In numerous cases, multiple narrow streams, in their travel, united and formed a wide dust plume (Fig. 4D), but some also continued as individual dust streams for hundreds of kilometers (Fig. 4C).

The length of the dust plumes reached values of 150 km to more than 600 km (Fig. 5). The areas covered by the dust plumes also varied from several thousand square kilometers to several hundreds of thousands of square kilometers. Air masses intruding from the east, northeast and southeast were observed to create the largest dust storm plumes.

4.2. Source areas of aerosol emissions by the TOMS and OMI AIs

Dust and sand storms have occurred over the Aral Sea region for thousands of years, but the accelerated shrinking of the sea in the 1970s resulted in important changes in dust storm frequencies, compositions and structures.

TOMS AI values highlighted the increasing importance of the Aral Sea's dried seabed, through time, as an active emission source of dust storms in the region (Fig. 6). The AI values showed that in the 1980s, the Aral Sea was a rather small, isolated source area of aerosols, with a slight increase of AI values in the last years of the decade. At the end of the 1980s, there were three main dried-out dust emission sources: one around the sea's northeastern shore, the second on Vozrojdenie Island and the third on the Kulandy Peninsula (Grigoryev and Jogova, 1992). According to TOMS, the most active dust source from 1980 to 1990 was on the eastern and southeastern dried sea bottom.

The ground data, prior to the year 2000, collected at the Aralsk Meteorological Station, which is situated in the northeastern region of the sea, showed that the northern part of the Aral Sea was a separate dust source area, affected seasonally by frequent dust storm outbreaks due to the expansion of the Aralkum Desert (Indoitu et al., 2012). The mean values of TOMS AI showed that the dust concentration in the atmosphere increased significantly by the end of the 1990s and the beginning of the 2000s (Fig. 6). The most active dust "hot spot," with the highest AI value (14), remained the eastern dried terraces. The AI average maps of the years 1997–2000 and 2000–2004 showed that the previous dust source area, isolated to the Aral Sea, spread spatially and created one large dust emission site that included the other dust source areas of the southern and northern deserts.

From the mean OMI AI (>1.0 indicates a greater concentration of aerosols in the atmosphere) values (Fig. 7), it is evident that the main dust emission area in Central Asia from 2005 to 2010 continued to be spatially distributed in the southern and northern

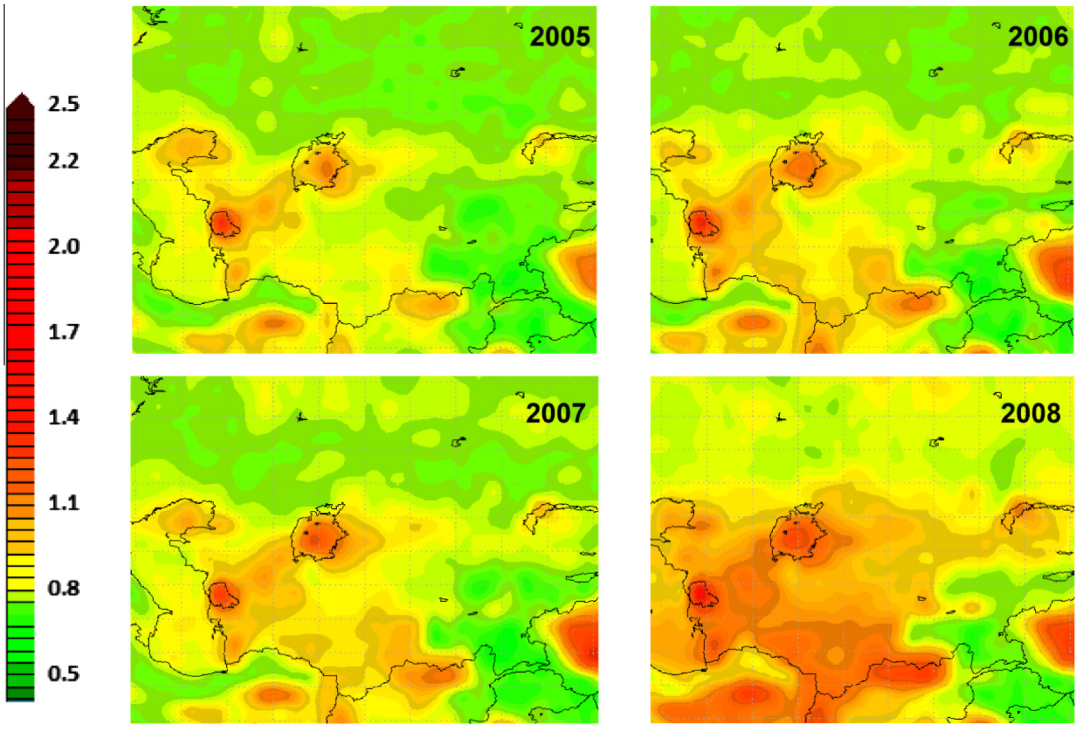

Fig. 9. OMI AI annual average for 2005–2008.

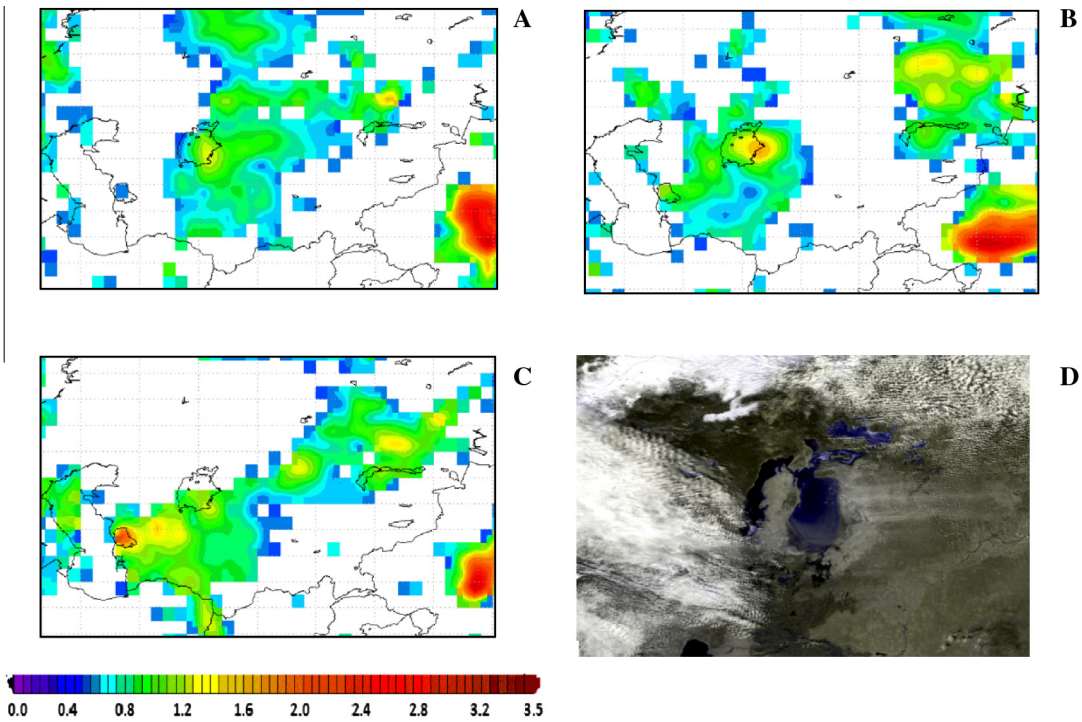

Fig. 10. OMI AI and NOAA-AVHRR for the dust event on March 18th 2005 (A) AI in March 17th 2005, (B) AI in March 18th 2005, (C) AI in March 19th 2005, (D) NOAA-AVHRR image of dust storm in March 18th 2005, band combination 2,2,1.

deserts. The TOMS AI showed that from March to September, the Aralkum Desert and the Karakum Desert, along with the areas adjacent to the southeastern Caspian shore, formed one large active dust storm zone. The higher OMI AI values showed that dust loadings originating from the Aralkum were carried hundreds of kilometers to the east and west (see Fig. 7).

4.3. Seasonality of dust storm activities from 2005 to 2008: using OMI AI

Previous ground data and satellite images showed that dust storms occur seasonally, with the maximum in the spring and summer (Indoitu et al., 2012). From 2005 to 2008, 14 (47%) dust

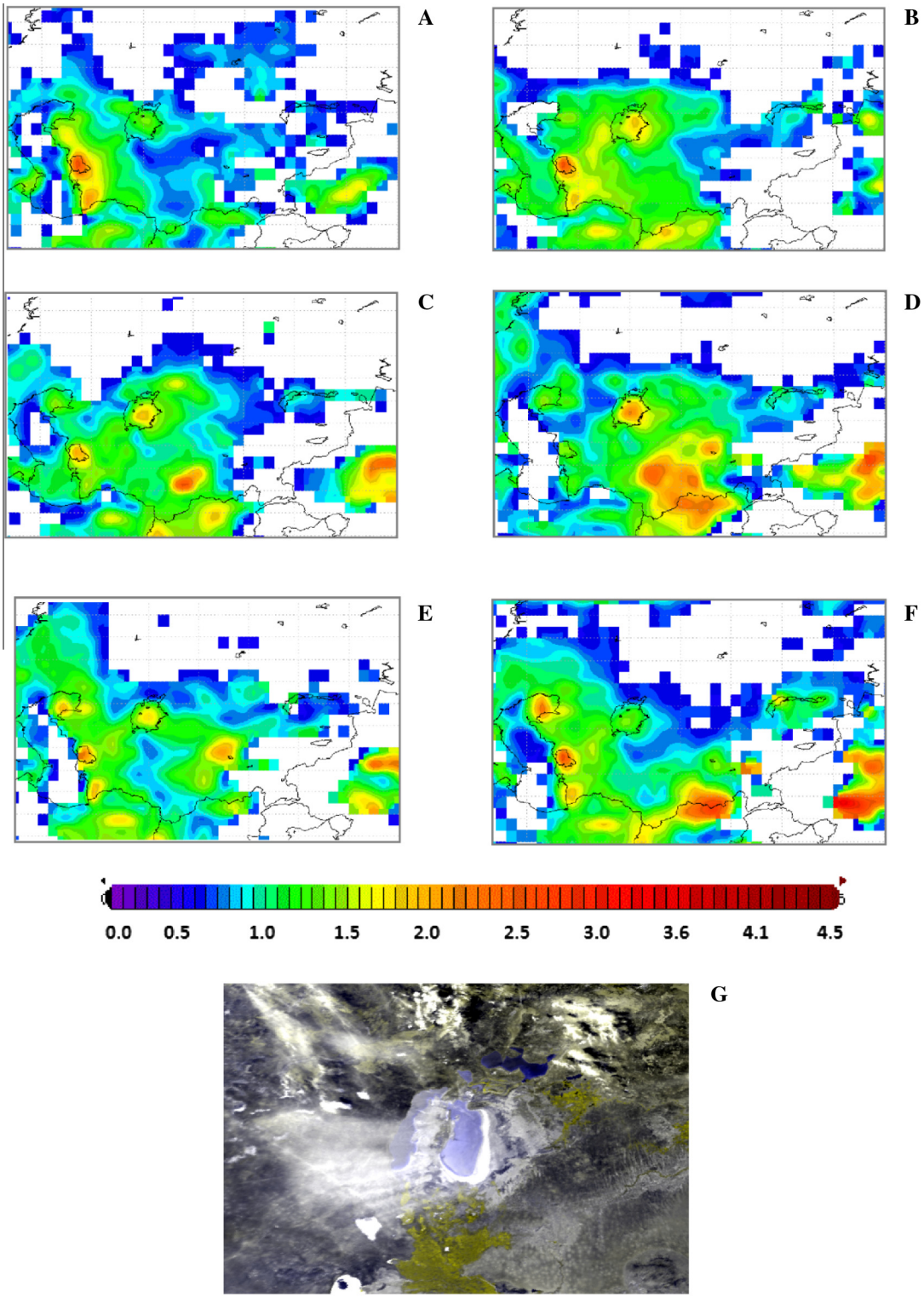

Fig. 11. OMI AI and NOAA-AVHRR for the dust storms on August 30th 2006 – September 2nd 2006 (A) AI in August 29th 2006, (B) AI in August 30th 2006, (C) AI in August 31st 2006, (D) AI in September 1st 2006, (E) AI in September 2nd 2006, (F) AI in September 3rd 2006, (G) NOAA-AVHRR image of dust storm in August 31st 2006, band combination 2,2,1.

storm events that occurred in April, seven (23%) in May, and three (10%) in March were observed using the NOAA AVHRR remote sensing imagery. Only two (7%) dust storm events were observed during June and July. During August–September, one dust storm event occurred in each month.

Monthly average AI maps, for the period 2005–2008, showed that the atmosphere between the Aralkum Desert and the deserts adjacent to the southeastern Caspian Sea shore was loaded with mineral aerosols from January to December. As the dust storm occurrence season began, the area affected by dust enlarged greatly. By April, mineral aerosol concentrations increased over separate smaller areas in the southern Karakum Desert. Later, from July through December, the OMI AI showed that the southern deserts and the Aral Sea region created one large dust source. In

general, during the year, the mean AI values over the Aral Sea didn't change at all, while the spatial distribution of the concentrated dust in the atmosphere enlarged significantly (Fig. 8) (the AI showed values of 1–1.5 for the entire year, on average).

AI values of 1–2 are characteristic of all dry lands affected by dust storms, with the exception being the Bodele Depression, Chad, which represents the largest site of dust storms, responsible for almost 40% of global mineralogical aerosols (AI = 2–4) (Prospero et al., 2002; Washington et al., 2003).

From the four years of observations, the OMI AI maps (Fig. 9) illustrated that the area under research was most affected by dust storms during 2008. Higher aerosol concentrations (1–1.5) covered the entire Karakum, Kyzylkum and Aralkum Deserts. During the four years, the mean maximum AI value (1.5–2) was registered only over a very small source point in the Kara Bogaz-Gol Gulf of the Caspian Sea. Only during 2008 were the AI values of 1.5–2 registered over a larger territory – covering the entire Kara Bogaz-Gol.

4.4. Case studies of dust storm events

A number of dust storm events, registered by NOAA AVHRR images, with dust transported to different directions, were correlated with the OMI AI.

In the last decades, a significant number of dust storms rising from the dried bottom of the Aral Sea were orientated to the eastern direction. A dust storm originating from the eastern shore close to the water line was observed on March 18, 2005 (Fig. 10). Dust was transported to a distance of more than 400 km, and the area of the dust plume was as large as 34,000 km^2 (see Fig. 5). The AI measured on the day before the event was 1.4 (Fig. 10A), and on March 18, 2005, it reached 1.7–1.8 (Fig. 10B). High concentrations of dust were observed the next day in the northern and central Kyzylkum Desert and the central Karakum Desert (Fig. 10C).

One of the most powerful dust events occurred in 2006 and lasted for four days, from August 30, 2006 till September 2, 2006 (Fig. 11). Dust started blowing in a westerly direction on August 30, mainly from the Vozrojdenie Island; on August 31 dust also raised up from the southern part of the dried bottom (which is a rather rare phenomenon). The dust storm reached its maximum on September 1 – the area of the dust plume was more than 110,000 km^2 with a length of more than 650 km (see Fig. 5). That day, dust originated from the eastern and southern shores and from Vozrojdenie Island. The next day, on September 2, the dust storm waned, and dust emitted from the eastern shore formed a narrow plume above the water surface, covering an area of about 22,000 km^2 and traveling a distance of 120 km. On August 30, an AI value of 1.8 was measured in the eastern part of the Aral Sea (Fig. 11A). The AI remained high the next day; high concentrations of dust were observed in the Karakum and Kyzylkum Deserts (Fig. 11B). On September 1, when the dust storm was at maximum, AI values reached 2.5–3 over the Aral Sea. The other "hot spot" was in the southeastern Karakum Desert and the southern Kyzylkum Desert (Fig. 11C). On September 2 the AI in the entire Circum-Aral region was between 1 and 1.7, and the dust front moved to the Caspian shore region (Fig. 11D).

Fig. 12 represents the strong dust storm caught with the NOAA AVHRR on May 9, 2007. The dust plume had a length of about 500 km and covered a surface of more than 113,000 km^2 (see Fig. 5). During this day, the AI registered values between 1.5 and 2.5, which covered the entire dried bottom of the Aral Sea. The OMI AI maps of the previous day and the day after the event showed that the dust storm was generated by a southern intrusion that swept the entire southern deserts. The air intrusion entered on May 8, 2007 from the south, covering the western part of the southern deserts, and on the next day, May 9, extended toward the east, thus covering the entire Karakum and Kyzylkum Deserts. The intrusion generated this massive dust storm on the dried bottom of the Aral Sea and probably also a smaller dust storm

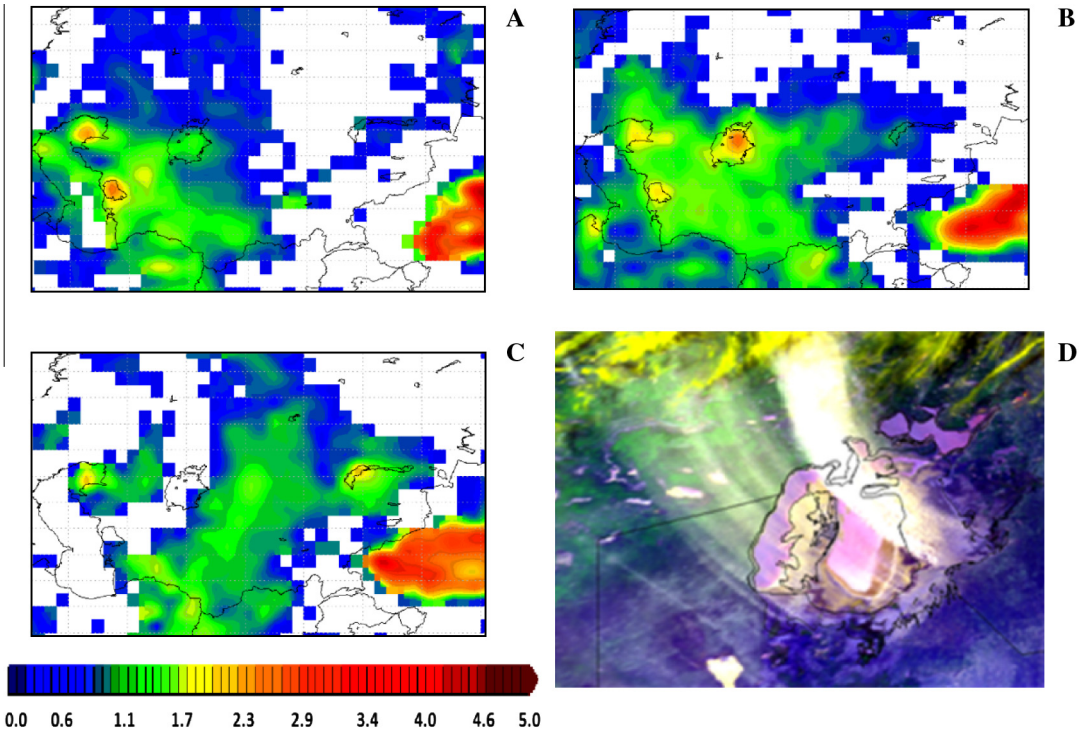

Fig. 12. OMI AI and NOAA-AVHRR for the dust event on May 09th 2007 (A- AI in May 08th 2007, B – AI in May 09th 2007, C – AI in May 10th 2007, D – NOAA-AVHRR image of dust storm in May 09th 2007, band combination 1,2,4).

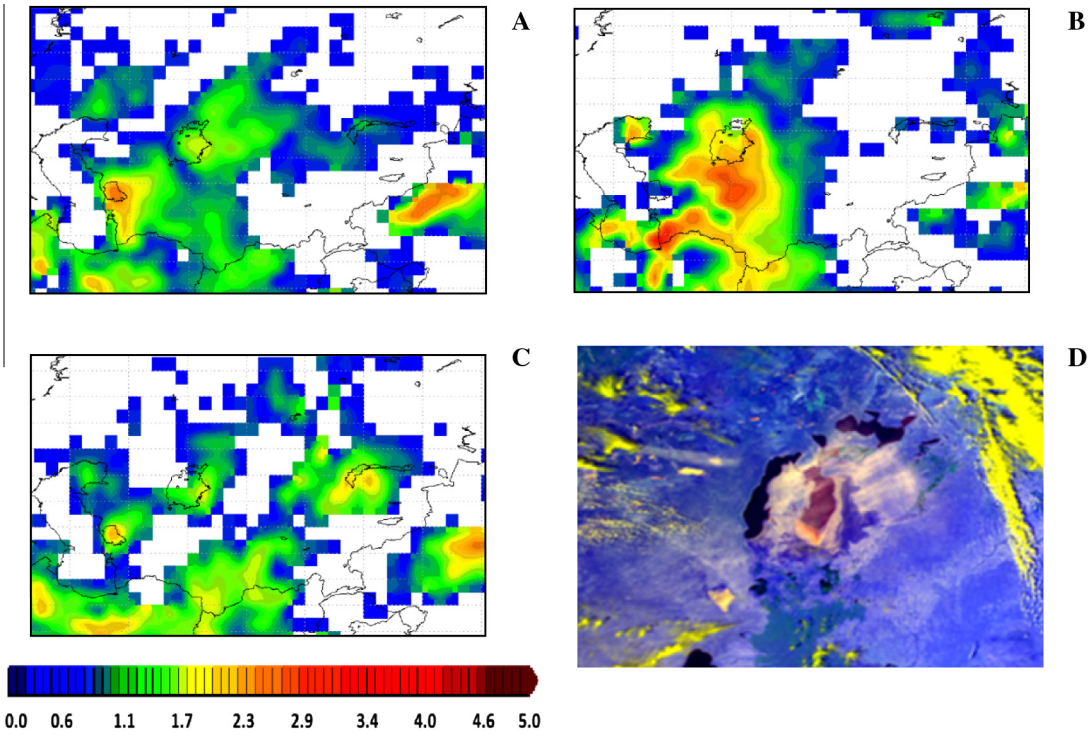

Fig. 13. OMI AI and NOAA-AVHRR for the dust event on May 28th 2008 (A) AI in May 27th 2008, (B) AI in May 28th 2008, (C) AI in May 29th 2008, (D) NOAA-AVHRR image of dust storm in May 28th 2008, band combination 1,2,4.

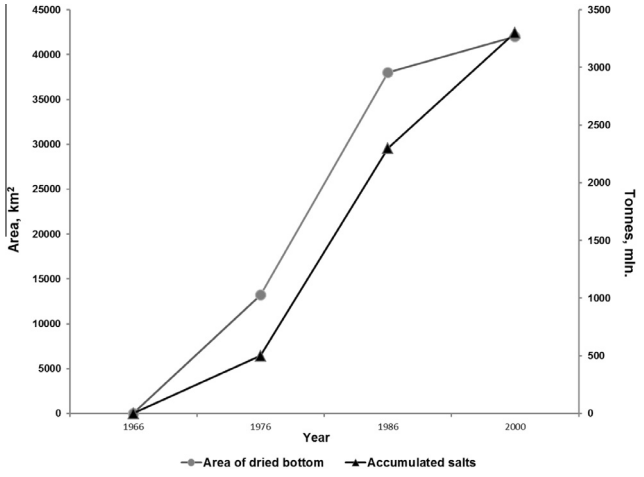

Fig. 14. Dynamics of the Aralkum Desert formation and amount of accumulated salts (after Rafikov and Kambarov, 2003).

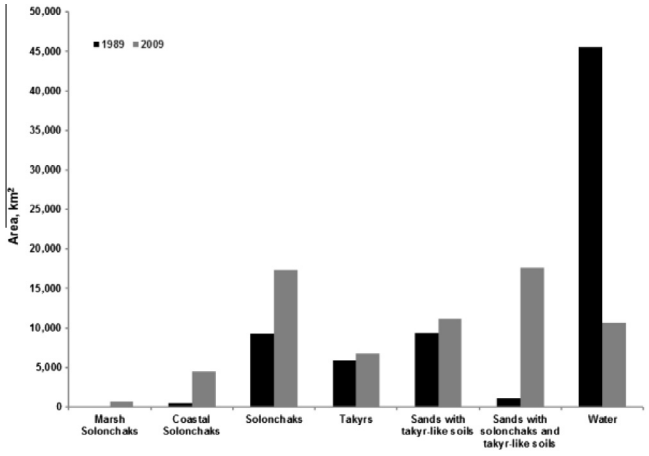

Fig. 15. Land cover changes in the Aralkum Desert in 1989–2009 (after Kozhoridze et al., 2012).

around the Aral Sea, as can be seen by the high OMI AI values that extended for large areas around the sea.

On May 28, 2008 (Fig. 13), a dust storm was captured, which was composed of multiple and small dust plumes, and compared to other dust storms, this one was a smaller event (see Fig. 5). The dust was blown from the entire dried sea bottom toward the northeast. The AI for this day showed high values for the eastern side of the Aral Basin (2.5) and about 3 for the southern shore.

The dust storm event of May 28, 2008, as in the previous example, was generated by a southern intrusion, which first covered the Karakum Desert and the southeastern Caspian shore, and during the next day, spread toward the east.

In general, the OMI Aerosol Index, calculated for the previous days, the day of the dust event and the day after the dust storm (see Figs. 10–13), showed that the dried bottom of the Aral Sea has become a separate powerful regional dust storm source. The AI values measured during dust storms increased from the dried bottom toward the south, west and east. The AI values during the dust storm outbreaks varied between 1.5 and 3.0, and were independent of the dust storm plume proportions.

4.5. Characteristics of the dust source sites on the dried Aral Sea bottom

As a result of the Aral Sea's desiccation since 1960, the newly formed Aralkum Desert has turned into an active source of dust with significant amounts of accumulated salts (Fig. 14) (Rafikov and Kambarov, 2003; Kuzmina and Novikova, 2008).

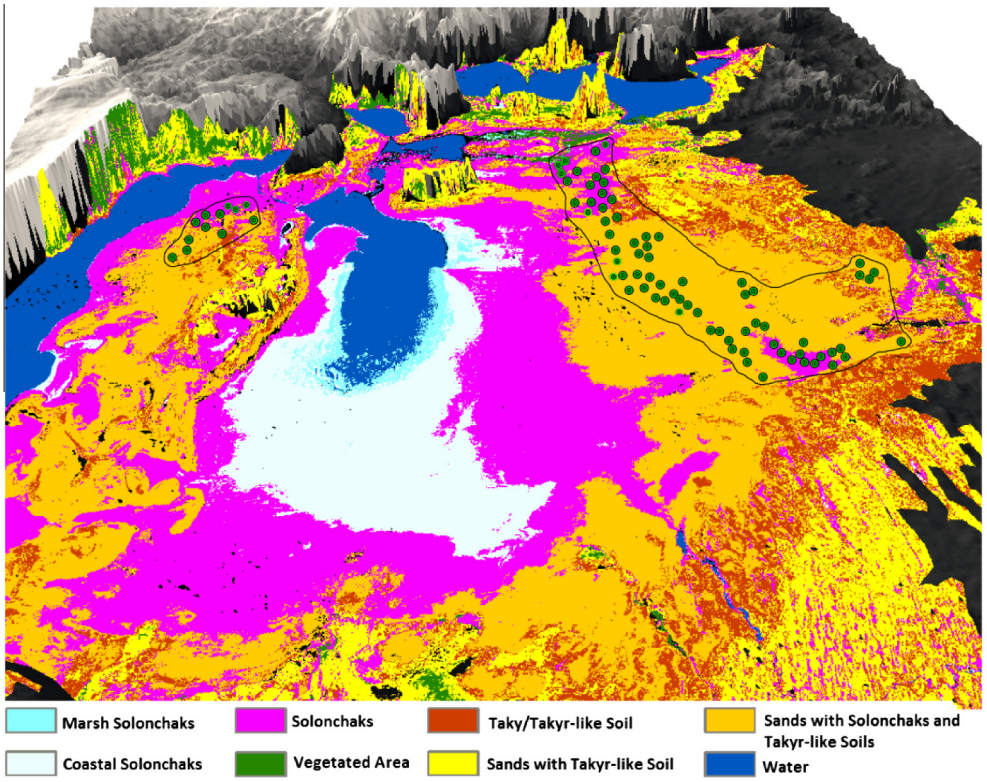

Fig. 16. 3D image with land cover classification of the dried bottom of the Aral Sea (after Kozhoridze et al., 2012); dots show the dust emission sites; contours show the active dust emission area in 2005–2008.

The land cover of the newly formed desert is characterized by high diversity. The salinity of the bottom deposits, as well as the types of the newly forming soils of the dried bottom, is an important factor in the development of the aeolian processes in the Aralkum Desert. In the northern and eastern parts of the former sea, heavier loamy deposits prevail, while in the southern and southeastern parts, lighter sandy and sandy-loamy ones are found (Starodubtsev and Bogdanetz, 2007). During the first decades of desiccation, the lighter bottom sediments were exposed, while in the last few years, this process has involved the heavier ones. As revealed by the recent studies, the exposed heavy takyr, takyr-like and solonchak surfaces have the highest potential for severe dust storms over the region (in the presence of sand fields in the nearby vicinity) (Singer et al., 2003). An analysis of the changes that have occurred in this area from 1989 to 2009 revealed an increasing area under these three land cover classes (Fig. 15) (Kozhoridze et al., 2012). The area of solonchaks (including marsh, coastal and dry solonchaks) expanded from about 10,000 km^2 in 1989 to 22,500 km^2 in 2009; the area occupied by sandy fields, in combination with takyr-like soils, increased from about 9500 km^2 in 1989 to almost 11,200 km^2 in 2009, and the complex of sandy massifs, solonchaks and takyrs grew during these two decades from 1000 km^2 in 1989 to 17,600 km^2 in 2009 (Kozhoridze et al., 2012). These findings are in a good agreement with the spatial distribution of dust emission sources demonstrated by the current study.

The digital elevation model of the dried bottom of the Aral Sea produced from www.worldclim.com and http://srtm.csi.cgiar.org/) was matched with a land cover classification of the same region compiled by Kozhoridze et al. (2012) (Fig. 16). The imposition of the contours of the active dust emission sites on the 3D image demonstrates that the main source of the dust from the Aral Sea's dried bottom are sandy massifs, combined with dry puffy solonchaks with easily destructible top surfaces, and takyrs. The active emission site consists of sands (75%), solonchaks (17%) and takyrs/takyr-like soils (8%).

5. Conclusions

This paper illustrates the dust storms status over the last decade and the ongoing processes in one of the most active dust- and salt-emitting sites in Central Asia. Additionally, an important task was to analyze the dust storm activity on the "old" dried bottom surface, which dried before the 1990s and has not been considered, in the last decades, as an active dust storm source due to the intensive colonization of the soil surface by plants.

The analysis of the NOAA AVHRR images showed that dust particles have been carried out from both the "older" and from the "newer" dried bottom of the sea. In most cases (70%), the dust plumes originated from the eastern terraces that dried before 1999. From 2005 to 2008, a large number of dust plumes had their origins on the surfaces dried before the 1990s, close to the 1960 water line.

The northeastern and eastern parts of the Aral Sea's dried bottom remain the main dust emission source; there was only one registered event where dust storm originated also from the southern part of the dried bottom.

As in the earlier observations, dust storms developed either as one large dust plume or as many small dust plumes. The large dust plumes, with widths between 60 km and 100 km, originated in the areas exposed before the 1990s. Small dust plumes usually rose from the "newer" dried areas, occupied by solonchaks. The distance of the dust transportation has also increased (compared to the remote sensing observations in the 1970s) – dust plumes often reach lengths of 150 km to more than 600 km.

An analysis of images for 2005–2008 showed that the main directions of the dust plumes' flow changed compared to the earlier

observations. From a total of 42 dust storm events extracted from the available NOAA AVHRR data, a small number of the dust storm events (14.3 %), originating from the eastern shore, were directed toward the east. This direction was not recorded in the previous observations. It was also observed that during the four-years period, 57.1% of the dust events were directed toward the west, 30% more than observed in the 1970s.

The TOMS and OMI AI highlighted how the shrinking of the Aral Sea has led to the development of a new and powerful source of dust storms in the region. The area of the Aral Sea in the 1960s was measured at about 66 000 km^2 with an average depth between 10 m and 60 m. By 2008, the water surface had vanished by approximately 80%.

Ground data collected before 1980 showed that dust events occurred mainly from May through September. The OMI AI showed that from 2005 to 2008, the atmosphere over the Aralkum Desert was loaded with mineral aerosols the whole year round – from January to December. During the year, the mean AI values over the Aral Sea didn't change, while the spatial distribution of the dust concentrations in the atmosphere and the dust sources increased significantly. According to the AI, the Aralkum Desert dust source, during the dust outbreaks, created one large dust source along with the Karakum and Kyzylkum Deserts. This could indicate that the dust storms in the late 2000s became more powerful and violent.

Land-cover changes were dominated by the expansion of the solonchaks and sandy massifs; these areas were the main sources of dust emission during the study period.

Due to the absence of meteorological and monitoring stations on the dried bottom of the Aral Sea, the only reliable source of information on the number of dust storm events, the emission sites and the direction of dust transport is remote sensing information.

Acknowledgements

This research was conducted under the support of the project "Long Term Ecological Research Program for Monitoring Aeolian Soil Erosion in Central Asia" (CALTER). The CALTER project was financed by the European Commission under the 6th Framework program for specific measures in support of international cooperation (INCO).

We wish to express our gratitude to the anonymous reviewer whose insightful comments helped to improve the quality of this manuscript.

References

Acker, J.G., Leptoukh, G. 2007. Online analysis enhances use of NASA earth science data, EOS, Trans. Am. Geophys. Union, 88(2) 14–17. (<http://disc.sci.gsfc.nasa.gov/giovanni/overview/how-to-acknowledge-giovanni>).

Ackerman, S.A., 1989. Using the radiative temperature difference at 3.7 μm and 11 μm to trace dust outbreaks. Remote Sens. Environ. 27, 129–133.

Ackerman, S.A., 1997. Remote sensing aerosols using satellite infrared observations. J. Geophys. Res. 102, 17069–17080.

Aladin, N.V., Plotnikov, I.S., Micklin, P., 2009. Aral Sea: water level, salinity and long-term changes in biological communities of an endangered ecosystem-past, present and future. Nat. Resour. Environ. Issues 15 (article 35).

Breckle, S., Wucherer, W., Dimeyeva, L., Ogar, N. (eds.), 2012. Aralkum – A man-made desert. The Desiccated Floor of the Aral Sea (Central Asia), Ecological Studies 218, Springer.

Chavez, J.P.S., Mackinnon, D.J., Reynolds, R.L., Velasco, M.G., 2002. Monitoring DS and mapping landscape vulnerability to wind erosion using satellite and ground-based digital images. Arid Lands Newsletter, (51).

Chiapello, I., Moulin, C., 2002. TOMS and METEOSAT satellite records of the variability of Saharan dust transport over the Atlantic during the last two decades (1979–1997). Geophys. Res. Lett. 29 (8), 1176. http://dx.doi.org/10.1029/2001GL013767.

Chiapello, I., Moulin, C., Prospero, J., 2005. Understanding the long-term variability of African dust transport across the Atlantic as recorded in both Barbados surface concentrations and large-scale Total Ozone Mapping Spectrometer (TOMS) optical thickness. J. Geophys. Res. 110, D18S10. http://dx.doi.org/10.1029/2004JD005132.

Dedova, T.V., Semenov, O.F., Tuseeva, N.B., 2006. Division of Kazakhstan territory by the repetition of very strong dust storms, and based on meteorological observations, remote sensing images and GIS (in Russian). Republic of Kazakhstan. Environment and Ecology. BOOK 3, 287–292.

Dosbergenov, C., Asanbayev, E., 2002. On aeolian salts carrying out from the dried bottom of the Aral Sea. Problems Desert Dev. 2, 37–42.

Dukhovny, V., Stulina, G., 2011. Water and food security in central Asia. NATO science for peace and security series C: environmental security, Springer.

Elguindi, N., Giorgi, F., 2007. Simulating future Caspian sea level changes using regional climate model outputs. Climate Dyn. 28, 365–379. http://dx.doi.org/10.1007/s00382-006-0185-x.

Engelstaedter, S., Tegen, I., Washington, R., 2006. North African dust emissions and transport. Earth Sci. Rev. 79, 73–100.

Evan, A., Heidinger, A., Pavolonis, M., 2006. Development of a new over-water Advanced Very High Resolution Radiometer dust detection algorithm. Int. J. Remote Sens. 27 (18), 3903–3924.

Fan Yi-da, S.P.-J., Ge Yi, Dou Wen, 2001. The analysis of typical DS in Northern china using remote sensing data. Adv. Earth Sci.

Galaeva, O.S., Idrysova, V.P. 2007. Climatic characteristics of dust storms in Circum-Aral region (Климатические особенности пыльных бурь приаралья). Scientific articles, Hydrometeorol. Ecol.

Glantz, M. 1999. Creeping environmental problems and sustainable development in the Aral Sea Basin.

Glantz, M., Figueroa, R., 1997. Does the Aral Sea merit heritage status? Global Environ. Change 7 (4), 357–380.

Glazovskiy, N.F. 1990. The Aral crisis: causative factors and means of solution (Aral'skiy krizis: prichiny vozniknoveniya i put' vykhoda). Nauka (20–23).

Grigoryev, A.A., Lipatov, V.B., 1974. Dust storms by data from satellite researches. Hydrometeoizda, Leningrad.

Grigoryev, A.A., Lipatov, V.B., 1982. Dynamics and sources of dust storms in the Aral region by satellite observations. In: Proceeding of the Academy of Sciences of the USSR, geographical series, 5, 93–98.

Grigoryev, A.A., Lipatov, V.B., 1983. Distribution of dust pollution in the Circum-Aral region by space monitoring. In: Proceeding of the Academy of Sciences of the USSR, geographical series, 4, 73–77.

Grigoryev, Al.A., Jogova, M.L., 1992. Strong dust blowouts in Aral region in 1985–1990. Proc. Russ. Acad. Sci. 324 (3), 672–675.

Hickey, B., Goudie, A., 2007. The use of TOMS and MODIS identify dust storm source areas: the Tokar delta (Sudan) and the Sistan basin (south west Asia), Prague.

Huang, J., Ge, J., Weng, F., 2007. Detection of Asia DS using multisensor satellite measurements. Remote Sens. Environ. 110, 186–191.

Hu, X.Q., Lu, N.M., Niu, T., Zhang, P., 2008. Operational retrieval of Asian sand and DS from FY-2C geostationary meteorological satellite and its application to real time forecast in Asia. Atmos. Chem. Phys. 8, 1649–1659.

Indoitu, R., Orlovsky, L., Orlovsky, N., 2012. Dust storms in Central Asia: spatial and temporal distribution. J. Arid Environ. 85, 62–70.

Jafari, R., Malekian, M., 2015. Comparison and evaluation of dust detection algorithms using MODIS Aqua/Terra Level 1B data and MODIS/OMI dust products in the Middle East. Int. J. Remote Sens. 36 (2), 597–617. http://dx.doi.org/10.1080/01431161.2014.999880.

Janugani, S., Jayaram, V., Cabrera, S.D., Rosiles, J.G., Gill, T.E., Rivera, N. 2009. Directional analysis and filtering for dust storm detection in NOAA-AVHRR imagery. Collection for University of Texas, E. P. P. A. ETD Collection for University of Texas, ed., El Paso.

Kaypov, I.V., Semenov, O.E., Shapov, A.P., 2012. Transportation of the aleurite aerosol from the dried bottom of the Aral Sea during the dust storm of April 28–29, 2008. Hydrometeorol. Ecol. 3, 7–30.

Khan, V.M., Vilfand, R.M., Zavialov, P.O., 2004. Long-term variability of air temperature in the Aral sea region. J. Mar. Syst. 47, 25–33.

Kondratyev, K., Grigoryev, A., Zhvalev, V., Melentyev, V., 1985. An integrated study of dust storms in the Aral region. Meteorol. Hydrol. 4, 32–38.

Kondratyev, K., Krapivin, V.F., Phillips, G.W., 2002. Global Environmental Change: Modelling and Monitoring. Springer, Heidelberg.

Kozhoridze G., Orlovsky L., Orlovsky N., 2012. Monitoring land cover dynamics in the Aral Sea region by remote sensing. In: Proc. SPIE 8538, Earth Resources and Environmental Remote Sensing/GIS Applications III, 85381V (October 25, 2012); http://dx.doi.org/10.1117/12.972306.

Kuzmina, Zh.V., Novikova, N.M., 2008. Monitoring of the vegetation in conditions of the Aral Sea ecological crisis. Russian Academy of Sciences, Water Problems Institute, Moscow, 29–39; 151–184.

Li, X., Ge, L., Dong, Y., Chang, H.-C., 2010. Estimating the greatest dust storm in eastern Australia with MODIS satellite images. Geosci. Remote Sens. Symp. (IGARSS).

Micklin, P.P., 1988. Desiccation of the Aral Sea: a water management disaster in the Soviet Union. Science 241, 1170–1176.

Micklin, P.P., 2010. The past, present, and future Aral Sea. Lakes Reservoirs Res. Manage. 15 (3), 193–213.

Miller, S.D., 2003. A consolidated technique for enhancing desert dust storms with MODIS. Geophys. Res. Lett. 30 (20), 2071. http://dx.doi.org/10.1029/2003GL018279.

NASA Earth Observatory, 2009. <http://earthobservatory.nasa.gov/>.

NESEDIS: NOAA Satellite, D. a. I. S. 2011. NOAA KLM User's Guide, Section 3.1. http://www2.ncdc.noaa.gov/docs/klm/html/c3/sec3-1.htm#top.

Novikova, N., 2004. Creeping Environmental Problems and Sustainable Development in the Aral Sea. Cambridge University Press.
Orlovsky, L., Orlovsky, N., 2001. White sandstorms in Central Asia. In: Global alarm: dust and sand storms from the world's drylands, 161–201.
Orlovsky, L., Tolkacheva, G., Orlovsky, N., Mamedov, B., 2004. Dust storms as a factor of atmospheric air pollution in the Aral Sea Basin. In: Brebbia, C.A. (Ed.), Air Pollution XII. WIT Press, Southampton, Boston, pp. 353–362.
Orlovsky, L., Orlovsky, N., Durdyev, A., 2005. Dust storms in Turkmenistan. J. Arid Environ. 60 (1), 83–97.
Perelet, R., 2008. Climate change in central Asia. UNDP.
Prospero, J.M., 1999. Long-range transport of mineral dust in the global atmosphere: Impact of African dust on the environment of the southeastern United States. Proc. Natl. Acad. Sci. U.S.A. 96, 3396–3403.
Prospero, J.M., Ginoux, P., Torres, O., Nicholson, S.E., Gill, T.E., 2002. Environmental characterization of global sources of atmospheric soil dust identified with the Nimbus 7 Total Ozone mapper Spectrometer (TOMS) absorbing aerosol product. Rev. Geophys. 40 (1), 2-1–2-31. http://dx.doi.org/10.1029/2000RG000095.
Putman, W. 2012. A dynamic portrait of global aerosols, SCCOMPANION, high performance computing, networking storage and analysis, SC Companion, pp. 1583–1588, http://dx.doi.org/10.1109/SC.Companion.2012.333.
Rafikov, V.A., Kambarov, R.K., 2003. A new Desert Aralkum. Problems Desert Dev. 1, 17–21.
Rivera, N.I., Bleiweiss, M.P., Hand, J.L., Gill, T.E. 2006. Characterization of dust storm sources in southwestern U.S. and northwestern Mexico using Remote Sensing imagery. In: Preprints, 14th Conference on Satellite Meteorology and Oceanography, Am. Meteorol. Soc., pp. P3.9, 17.
Roskovensky, J.K., Liouand, K.N., 2005. Differentiating airborne dust from cirrus clouds using MODIS data. Geophys. Res. Lett. 32 (L12809).
Saiko, T., Zonn, I.S., 2000. Irrigation expansion and dynamics of desertification in the Circum-Aral region of Central Asia. Appl. Geogr. 20, 349–367.
Shardakova, L.U., Usmanova, L.V., 2006. Analysis of dust storms in the Circum-Aral region. Prob. Desert Dev. 3, 30–34.
Semenov, O.E., 2011. Introduction to experimental meteorology and climatology of dust storms. Almaty, pp. 580, ISBN 978-601-278-528-9.
Singer, A., Zobeck, T., Poberezsky, L., Argaman, E., 2003. The PM10 and PM2.5 dust generation potential of soils/sediments in the Southern Aral Sea Basin, Uzbekistan. J. Arid Environ. 54 (4), 705–728.
Singh, A., Seitz, F., Schwatke, C., 2012. Inter-annual water storage changes in the Aral Sea from multi-mission satellite altimetry, optical remote sensing, and GRACE satellite gravimetry. Remote Sens. Environ. 123, 187–195.
Sokolik, I., 2002. The spectral radiative signature of wind-blown mineral dust: Implications for remote sensing in the thermal IR region. Geophys. Res. Lett. 29 (24), 2154. http://dx.doi.org/10.1029/2002GL015910.
Sorg, A., Bolch, T., Stoffel, M., Solomina, O., Beniston, M., 2012. Climate change impacts on glaciers and runoff in Tien Shan (Central Asia). Nat. Clim. Change 2, 725–731.
Spivak, L., Terekhov, A., Vitkovskaya, I., Batyrbayeva, M., 2009. Analysis of changes of the zone of formation of salt-dust storms from the drained bottom of the Aral Sea with using the long-term satellite data. Curr. Prob. Remote Sens. Earth Space 2 (6), 193–202.
Spivak, L., Terechov, A., Vitkovskaya, I., Batyrbayeva, M., Orlovsky, L. 2012. Dynamics of dust transfer from the desiccated Aral Sea bottom analyzed by remote sensing. In: S. Breckle, W. Wucherer, L. Dimeyeva, N. Ogar (eds.) Aralkum – A man-made desert. The Desiccated Floor of the Aral Sea (Central Asia), Ecological Studies 218, Springer.
Starodubtsev, V.M., Bogdanetz, V.A., 2007. Formation of the soil cover on the dried bottom of the Aral Sea. Prob. Desert Dev. 3, 34–40.
Tsolmon, Ochirkhuyag, L.R., Sternberg, T., 2008. Monitoring the source of trans-national DS in north east Asia. Int. J. Digital Earth 1 (1), 119–129.
Washington, R., Bouet, C., Cautenet, G., Mackenzie, E., Ashpole, I., Engelstaedter, S., Lizcano, G., Henderson, G., Schepanski, K., Tegen, I., 2009. Dust as a tipping element: The Bodélé Depression, Chad. PNAS 106, 20564–20571.
Washington, R., Todd, M., Middleton, N.J., Goudie, A.S., 2003. Dust-Storm Source Areas Determined by the Total Ozone Monitoring Spectrometer and Surface Observations. Ann. Assoc. Am. Geographers 93 (2), 297–313.
Wiggs, G.F., O'Hara, S.L., Wegerdt, J., Van Der Meer, J., Small, I., Hubbard, R., 2003. The dynamics and characteristics of aeolian dust in dryland Central Asia: possible impacts on human exposure and respiratory health in the Aral Sea basin. Geog. J. 169 (2), 142–157.